

# Isolation enhanced MIMO PIFA system with multiple reconfiguration techniques

ISSN 1751-8725  
 Received on 20th June 2019  
 Revised 12th January 2020  
 Accepted on 27th January 2020  
 E-First on 15th April 2020  
 doi: 10.1049/iet-map.2019.0547  
 www.ietdl.org

Fatima A. Asadallah<sup>1</sup> ✉, Joseph Costantine<sup>1</sup>, Youssef Tawk<sup>1</sup>

<sup>1</sup>Electrical and Computer Engineering Department, American University of Beirut, Beirut 1107 2020, Lebanon

✉ E-mail: fba16@mail.aub.edu

**Abstract:** In this study, a reconfigurable, two-element, multiple-input multiple-output (MIMO) printed inverted-F antenna (PIFA) is presented with an enhanced isolation ability. The MIMO antenna system is designed using three different reconfiguration techniques that are based on positive-intrinsic-negative diodes, radio frequency micro-electromechanical switches and varactors. Their impact on the performance of the PIFA and the MIMO system is evaluated in terms of radiation characteristics, gain, power dissipated, radiation efficiency, linearity, biasing requirements and MIMO performance. Isolation between the two MIMO antenna elements is enhanced by integrating a reconfigurable band-reject filter within the ground plane between the radiating elements. The band-reject filter is reconfigured simultaneously with the radiating elements, hence resulting in less coupling and better isolation. The MIMO system along its various components is fabricated for the three different reconfiguration techniques and the comparison with predicted data shows great agreement.

## 1 Introduction

With the rapid development of wireless communication systems, and the rise of internet of things (IoT), the requirements on communication systems are increasing significantly. In fact, RF front-end systems will be responsible for the communication needs of more than 75 billion devices in 2025 as reported in [1]. Therefore, designers and researchers are seeking compact antenna systems that cater for the pressing wireless communication needs. With the addition of needed antennas, a higher caliber of isolation is required between the various elements. On the other hand, reconfigurable antenna systems present a solution that mitigates strong signal interference and copes with the changing environmental conditions. Reducing the size of these antennas and their integration as part of dynamic multiple-input multiple-output (MIMO) systems present a suitable solution. In reality, the reconfiguration of an antenna results in a change in its operating frequency, radiation pattern or polarisation scheme. Electrical switches, mechanical actuators and other techniques are considered to achieve such reconfiguration [2–9]. Electrical switches are the most popular components that are incorporated on antenna structures to achieve reconfiguration [2–8]. Examples of electrical switches are positive-intrinsic-negative (PIN) diodes [3–6], varactors [7] or radio frequency micro-electromechanical switches (RF-MEMS). However, literature lacks the analysis of the impact of such reconfiguring components on the antenna performance, especially in a MIMO environment.

Integrating a reconfigurable antenna within a MIMO system contributes through an added agility to the performance of the MIMO system. A major challenge to MIMO antenna systems is based on ensuring a high level of isolation between the various radiating elements [10–16]. Such isolation is instrumental in a communication system that relies on a multitude of antenna components to satisfy the needs of a rich communication environment. Several MIMO antenna designs are investigated and presented in literature [10–16] where various techniques are proposed to improve the isolation between the different antenna elements. One of the techniques used is based on inserting isolators between the antenna elements [10]. This technique requires additional space for the isolator which adds complexity to the overall system. Other techniques include inserting coupled-line resonator, interdigital lines, capacitive load loops and others [11–16].

The work presented in this paper introduces a new reconfigurable, two-element, MIMO system that relies on different switching techniques to dynamically operate at various applications with an enhanced isolation. The MIMO systems are analysed in detail and compared in terms of their radiation characteristics. The antenna elements composing the MIMO systems are based on reconfigurable printed inverted-F antenna (PIFA) topologies. The PIFA elements are first reconfigured by relying on PIN diodes, RF MEMS or varactors in order to cover all the needed frequencies of operation over mobile and compact terminals. The original presentation of the PIFA component topology discussed in [17, 18] does not take into consideration their reconfiguration ability. Enhancing the isolation between the antenna elements is achieved by simultaneously reconfiguring a ground-integrated-band-reject filter between the PIFA components. This reconfigurable isolation between the elements is far more enhanced in comparison to a static multiband reject filter [19] or any static isolating component. Such advantageous dynamic isolation advances the user's needs in a rich communication environment.

The novelty of the work presented in this paper is based on the analysis of the effects of the various reconfiguration techniques on the PIFA radiation characteristics. This is to our knowledge the first time that such analysis is executed across a reconfigurable MIMO system with a multitude of reconfiguration techniques. In fact, the focus of this paper is to evaluate the impact of PIN diodes, RF-MEMS and varactors on the gain, power dissipated, radiation efficiency, linearity and biasing requirements of the MIMO systems. Such analysis allows antenna designers to always commit to an informed decision on the reconfiguring component's choice. Another aspect is the integration of a reconfigurable band reject filter in the ground plane of a reconfigurable MIMO PIFA. The band reject filter is reconfigured by relying on the same reconfiguration techniques implemented within the radiating elements. Thus, for every reconfiguration state of the filter, the radiating elements operate at the same frequencies of interest. The band rejection of the filter is coordinated and reconfigured at the same instance as the radiating elements. Such reconfigurable isolation enhances the overall MIMO performance.

Novelty can also be identified in the compact MIMO implementation where the two antenna elements are integrated in close proximity and still meet the rigid MIMO criteria. This is due to the fact that the band reject filter exhibits the same slot topology as that of the radiating elements with simultaneous reconfiguration.

**Table 1** Comparative table presenting the novelty aspects of this paper versus previously published ones

Novelty aspects	[17]	[18]	[19]	Proposed work
multiband PIFA element design	X	X		
reconfigurable PIFA element design using single reconfiguration techniques	X	X	X	X
reconfigurable PIFA design using variety of reconfiguration techniques				X
analysis and comparison of the PIFAs radiation characteristic by relying on different configuration techniques				X
design and analysis of reconfigurable band reject filter based on DGS using different reconfiguration techniques				X
reconfigurable MIMO PIFA system with multiband reject filter for isolation enhancement			X	X
reconfigurable MIMO PIFA system with reconfigurable band reject filter for isolation enhancement				X
design and analysis of the full MIMO PIFA system using the reconfigurable isolation enhancement technique with different switching techniques				X
analysis and comparison of the full MIMO system's radiation characteristic by relying on different configuration techniques				X

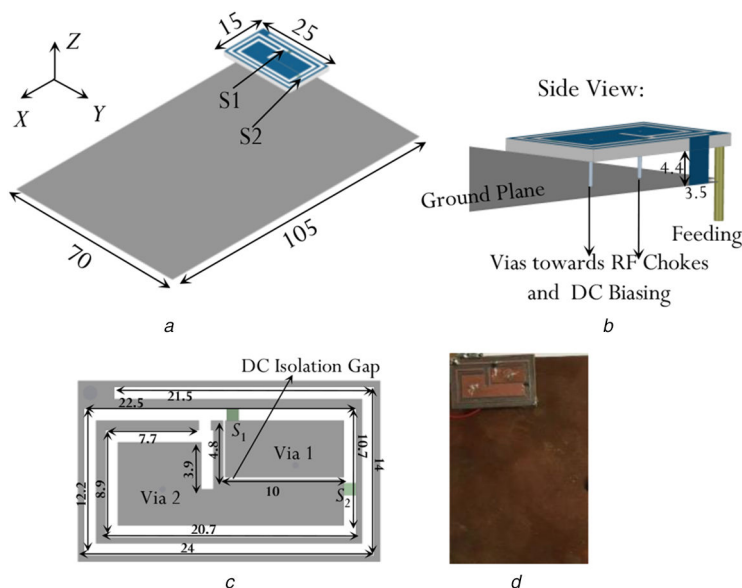
**Fig. 1** Reconfigurable PIFA structure along with its fabricated prototype  
(a) 3D view of the antenna, (b) Side view of the antenna, (c) Detailed dimensions of the patch, (d) Fabricated prototype

Table 1 summarises the differences between the work presented in this paper and the authors' previously published work that is related to the PIFA integration.

Section 2 of this paper discusses the reconfigurable PIFA structure that is reconfigured using either PIN diodes, RF-MEMs or varactors. Section 3 presents a detailed analysis and a comparative study between the different reconfiguring components and their effects on the systems' performance. Section 4 presents the MIMO system that includes a reconfigurable isolating band reject filter within its ground plane. In addition, Section 4 details the improvement in isolation between the radiating elements and the impact of the various reconfiguration techniques on the MIMO performance. Section 5 concludes the paper.

## 2 PIFA design using different reconfigurable components

### 2.1 PIFA design using pin diodes

The proposed PIFA structure is composed of a rectangular patch with dimensions of  $25 \times 15 \text{ mm}^2$ . The patch is based on Rogers Duroid 5880 substrate with a dielectric constant of 2.2 and a thickness of 1.6 mm. The substrate is suspended away from the ground plane by 4.4 mm. The antenna's ground plane is taken to represent the size of a typical mobile phone and is considered to have an overall dimension of  $105 \times 70 \text{ mm}^2$  as shown in Fig. 1a. A shorting sheet of width 3.5 mm is incorporated at a distance of 2 mm from the feeding point as shown in Fig. 1b. The patch and shorting sheet are designed such that the sum of the length and

width of the patch subtracted by the shorting sheet width is equal to  $34.5 \text{ mm}$  ( $\lambda/4$  at 1.8 GHz) [20].

One capacitive slot is etched from the rectangular patch that has the length of  $\lambda/2$  at 900 MHz. The slot's topology has an almost rectangular spiral shape as shown in Fig. 1c. Such topology ensures better compactness for the antenna's radiating surface. Two switches (S1, S2) are mounted on the slot at strategic optimised locations to achieve the required frequency reconfiguration. The first incorporated switches in this work are SMP 1320-079LF PIN diodes [21]. The different switches' states allow the variation of the slot's length and hence enable the antenna to reconfigure its frequency operation. The pin diodes can be biased separately due to the etching of a direct current (DC) isolation gap that is shown in Fig. 1c. Two 110 nH L-07WR11KV4 T [22] RF chokes are introduced through vias at optimised locations to connect the pin diodes to the DC power supply. The RF chokes prevent RF leakage from the antenna towards the DC biasing circuit. The location of the RF chokes as well as the shorting pins are studied to minimise their impact. Hence, they are connected through vias as indicated in Fig. 1b. The integrated switches get their connections to the ground plane through the shorting sheet of the PIFA structure. The fabricated prototype of the single element reconfigurable PIFA is presented in Fig. 1d. The antenna's reflection coefficient is measured by a vector network analyser from Keysight [23].

Fig. 2 shows the comparison between the measured and simulated reflection coefficient of the reconfigurable design for different combinations of the PIN diodes' states. The antenna covers the following frequencies (770 MHz, 900 MHz, 1.54 GHz, 1.8 GHz, 2.1 GHz and 2.4 GHz) for different modes of operation of the two integrated switches. These frequencies allow the antenna to

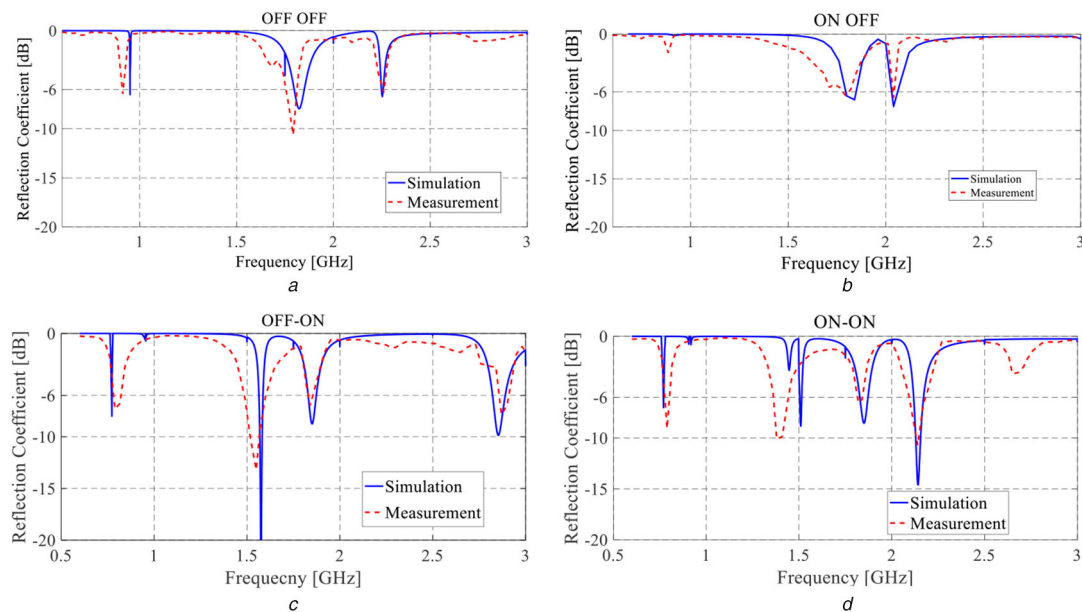


**Fig. 2** Simulated and measured reflection coefficient in dB for different switches configurations using pin diodes  
 (a) OFF–OFF state, (b) ON–OFF state, (c) OFF–ON state, (d) ON–ON state

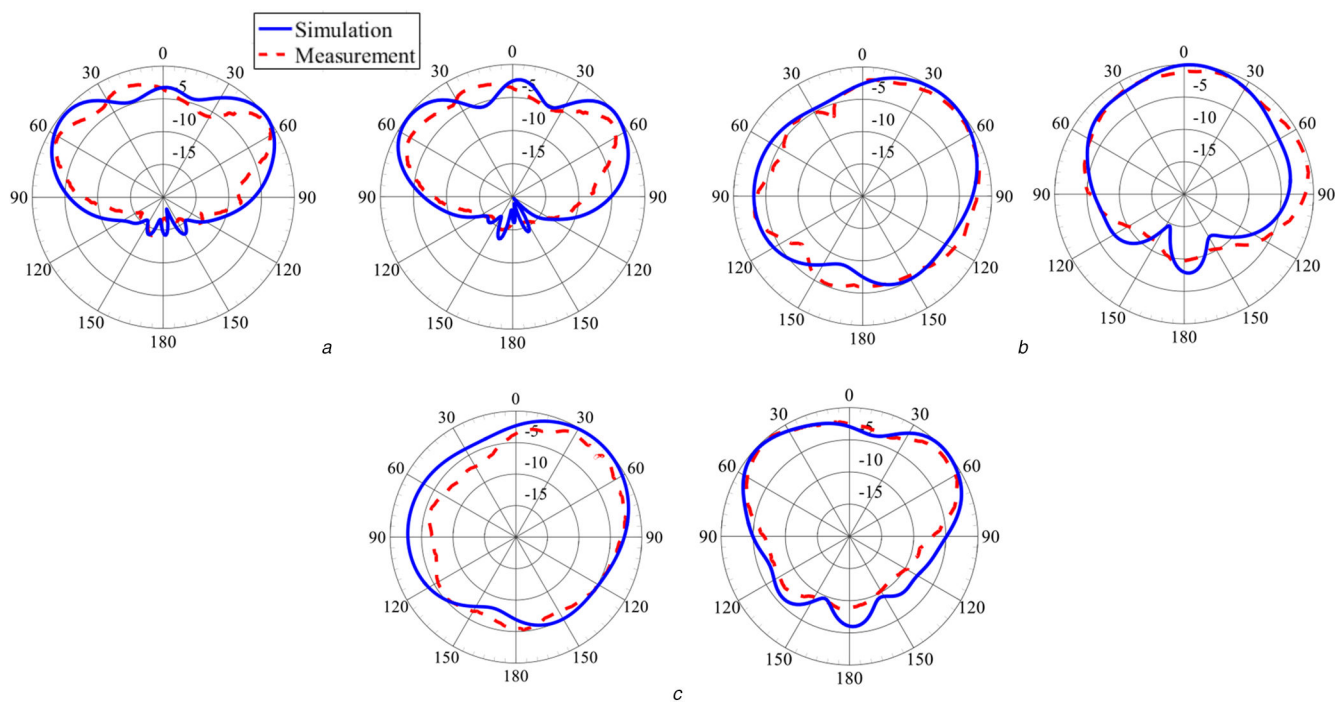


**Fig. 3** Simulated and measured radiation pattern of the reconfigurable PIFA for  $\varphi = 90^\circ$  at  
 (a) 1.8 GHz when S2 is ON, 2.1 GHz when S1 is ON, (b) 900 MHz when M1 is ON, 1.8 GHz when M2 is ON, (c) 900 MHz when the varactor has an equivalent capacitance of 0.94 pF and 1.8 GHz when the varactor has an equivalent capacitance of 0.74 pF

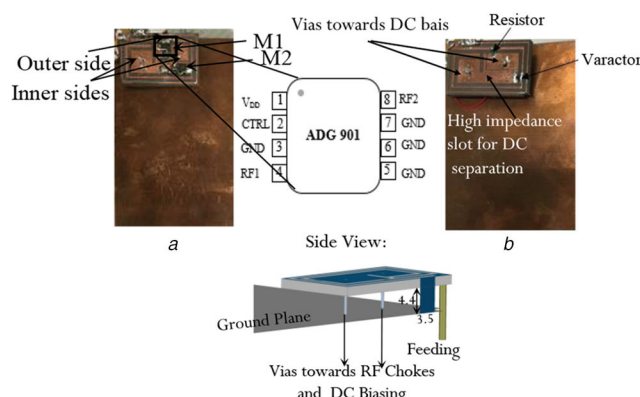
operate at various wireless communication applications such as LTE, GSM, GPS, 3G and Wi-Fi. The antenna's radiation pattern, gain and radiation efficiency are measured in an ETS-Lindgren anechoic chamber [24] in the antenna measurement laboratory on campus. Figs. 3a and b represent the comparison between the measured and simulated radiation patterns at 2.1 GHz when the PIN diode switch S1 is ON and 1.8 GHz when the PIN diode switch S2 is ON. The antenna's simulated and measured maximum realised gains for various configurations and various frequencies as well as the antenna's radiation efficiency along with the RF power dissipated at the various operating frequencies are presented in Table 2. The antenna's operating bandwidth for each band is also summarised in Table 2.

## 2.2 PIFA design using RF MEMS

In order to investigate and study the effect of the reconfiguring component on the performance of the reconfigurable antenna, the same antenna structure is re-designed using RF-MEMS. The antenna is integrated into the simulation environment with RF-MEMS instead of PIN diodes, where the locations of the switches remain the same. The fabricated prototype is shown in Fig. 4a. Two ADG901 MEMS [25] along with their respective biasing networks and a shorting sheet are integrated within the antenna to ensure a successful frequency reconfigurable operation. The control circuitry (DC bias, RF chokes and control bias) is illustrated in Fig. 1b and Fig. 4. The same RF chokes, vias and DC biasing lines presented in Fig. 1b are used to bias the RF MEMS or the varactor. This switch is an eight-pin analogue device. Its pin configuration is shown in Fig. 4a. The RF supply pin 1 (RF<sub>1</sub>) and

**Table 2** Operating frequencies for various switches configurations along with the corresponding maximum gains, radiation efficiencies and RF power dissipated for pin diodes

Switch state	Operating freq., GHz	Bandwidth, MHz	Max. gain, dB		Radiation efficiency, %		Power dissipated, dBm
			Simulated	Measured	Sim.	Meas.	
S1 OFF and S2 OFF	0.9	10	0.5	0.45	32	28	5.6
	1.8	50	4	3.7	15	12.5	12.6
	2.4	20	4	3.8	17	16	11.6
S1 OFF and S2 ON	0.77	10	0.5	0.5	40	38	4.3
	1.54	30	1	0.98	30	28	6.1
	1.8	40	4	3.82	14	12.5	12.7
	2.66	70	4	3.9	16	14	12.2
S1 ON and S2 OFF	1.8	40	4	3.9	12.5	12.3	12.8
	2.1	30	3.5	3.37	25	24.5	9.2
S1 ON and S1 ON	0.77	10	0.5	0.5	38	37.5	8.9
	1.54	30	1	0.98	28	27	6.1
	1.8	40	4	3.9	11	10	17
	2.1	30	3.5	3.37	22	20	12

**Fig. 4** Reconfigurable PIFA structure (a) Using RF-MEMS, (b) Using varactor

the DC supply pin ( $V_{DD}$ ) are connected to the inner side of the antenna. This side of the antenna is connected through vias to a 110 nH L-07WR11KV4 T inductor that prevents the leakage of the RF signal back to the DC power source. The ground (GND) pins and the  $RF_2$  pin are connected to the outer side of the antenna. The CTRL pin is connected to  $V_{DD}$  when the RF-MEMS is operating in the ON state. When the RF-MEMS is OFF, it is connected to GND.

Two RF-MEMS can guarantee four states of operation. Similar to the case of pin diodes, three states are sufficient to achieve the required bands of operation (770 MHz, 900 MHz, 1.54 GHz, 1.8 GHz, 2.1 GHz and 2.4 GHz). Fig. 5 shows the comparison of the reflection coefficient results between the simulation and measurement for the various states of the switches where a good agreement is observed. The smaller magnitudes of the reflection coefficients for RF MEMS in comparison to the pin diodes' configurations are due to the different capacitance and resistance values of the switches. Some minor discrepancy between measured and simulated reflection coefficient results as displayed in Fig. 5d is expected due to the natural fabrication errors, measurement instrumentation maintenance, distortion, non-linearity of components and ambient noise. The simulated and measured maximum realised gains and radiation efficiencies at the various frequencies of operation are displayed in Table 3. This table also includes the operating bandwidth and RF power dissipated for various states of the two RF-MEMS.

The measured gain levels range from 0.2 to 4.3 dB for various frequencies at different configurations. The variation is due to the different current distributions at various frequencies. It can be noticed that the radiation efficiency and the RF power dissipated in this case are better than that of pin diodes. The comparison between measured and simulated radiation patterns at 900 MHz and 1.8 GHz are shown in Figs. 3c and d.

### 2.3 PIFA design using varactors

Designing a reconfigurable antenna using varactors forces the designer to consider their tunable capacitance. Implementing such components on a reconfigurable PIFA instead of PIN diodes or RF-MEMS adds tuning ability to the antenna design and alters its performance. In reality, the tunable capacitance value also leads to frequency tuning and can provide reconfiguration to the antenna design. After analysis, it is found that the required reconfigurable antenna functionality can be achieved with only one varactor and one resistor.

Hence, the number of switching components can be reduced, which impacts the biasing requirements as well. The antenna structure shown in Fig. 4b relies on the SMV1247-079LF varactor [26]. Its capacitance changes from 8.86 to 0.64 pF with a varying input voltage. This variable capacitance enables frequency tuning and allows the antenna to cover the required bands. A comparison between the simulated and measured reflection coefficients is shown in Fig. 6. It is important to note that Fig. 6 shows some discrepancy between the simulation and measurement. This difference is expected due to the natural fabrication errors, measurement instrumentation maintenance, distortion, non-linearity of components and ambient noise. Table 4 represents the bandwidths covered upon tuning the capacitance values of the varactor. Also, Table 4 presents the measured and simulated peak gain values of the PIFA for the different operating frequencies. The gain ranges between 1.1 and 4.5 dB. Good performance is observed for the various states of the varactor. In addition, Table 4 shows the radiation efficiency and RF power dissipated in the antenna design for various varactor capacitances. It is noticed that by relying on a varactor, the antenna tunes its operational bandwidths and thus covers all the required uplink/downlink channels for the desired applications. This performance advantage lacks from the case of integrated PIN diodes and RF MEMS. In addition, the radiation

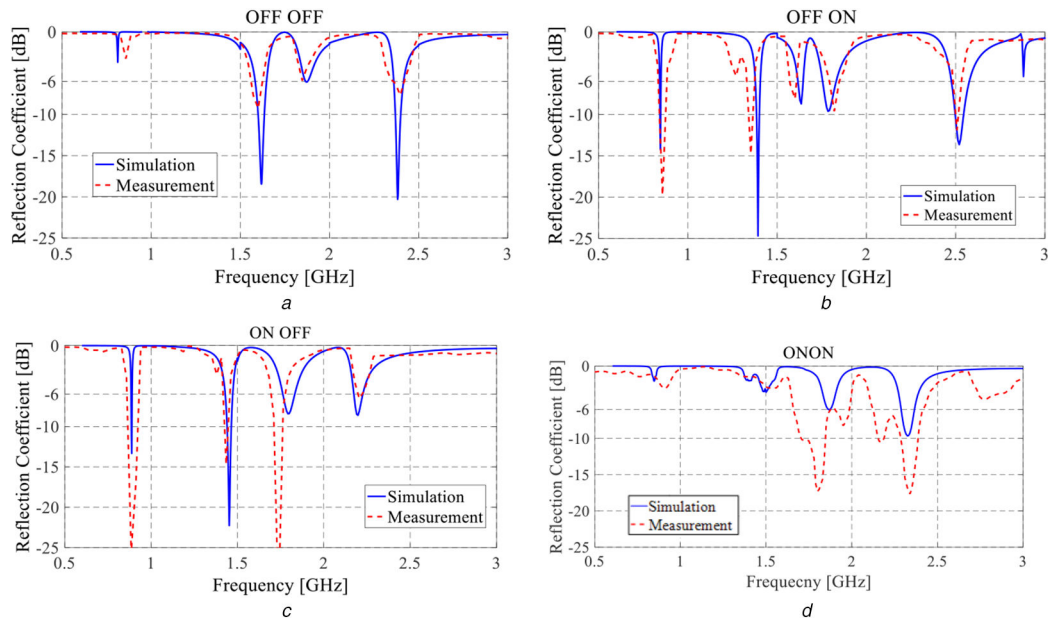


**Fig. 5** Simulated and measured reflection coefficient in dB for the various states and biasing conditions of the RF MEMS  
(a) OFF-OFF state, (b) OFF-ON state, (c) ON-OFF state, (d) ON-ON state

**Table 3** Operating frequencies for various switches configurations along with the corresponding maximum gains, radiation efficiencies and RF power dissipated for RF MEMS

Switch state	Operating freq., GHz	Bandwidth, MHz	Max. gain, dB		Radiation efficiency, %		Power dissipated, dBm
			Simulated	Measured	Sim.	Meas.	
M1 OFF and M2 OFF	1.54	20	4.5	4	95	93	4.2
	2.4	100	5.1	5	95	93	5.2
M1 OFF and M2 ON	0.77	10	0.4	0.37	61	63	2.3
	1.54	20	2.72	2.9	78	78	3.8
	1.8	40	4.6	4.3	95	93	4.5
	2.66	90	4.5	4.3	97	93	4.5
M1 ON and M2 OFF	0.9	12	0	0.2	48	50	3.1
	1.54	40	2.8	2.1	73	72	3.4
	1.8	70	4.1	4.07	88	85	4.7
	2.1	60	3.7	3.5	78	73	4.7
M1 ON and M2 ON	1.8	30	2	2	90	89	7
	2.4	70	4.29	4	83	80	7

efficiency of the antenna and the RF power dissipated in this case is better than that of pin diodes and RF MEMS. The radiation patterns at 900 MHz when the varactor has an equivalent capacitance of 0.94 pF and 1.8 GHz when the varactor has an equivalent capacitance of 0.74 pF are presented in Figs. 3e and f where good agreement is achieved between the simulation and measurement.

### 3 Impact of switches' integration on the design and characteristics of the reconfigurable PIFA

The choice of the reconfiguring component to be integrated within the antenna structure impacts the performance of the antenna and its radiation characteristics. It also impacts the design process of the antenna itself as discussed in the previous sections. In this section, the effects of the various integrated switches onto the design and performance of the presented reconfigurable PIFA is detailed.

#### 3.1 Number of switches

In this PIFA design, two PIN diodes and two RF MEMS are needed to achieve the desired operation at the needed wireless communication applications. However, only one varactor is sufficient to reach the desired frequencies.

#### 3.2 Biasing

The three types of switches analysed in this paper require analogue input power for biasing. For the PIN diode to operate in the ON state, it requires a voltage of 1 V with a 10 mA current resulting in 10 mW DC input power. The used RF-MEMS require 2.2 V with 78 mA current and thus 171 mW DC input power. However, in the case of varactors the voltage needed reaches 8 V and thus 250 mW dissipated power. Therefore, the reconfiguring component requiring less DC input power is the PIN diode, followed by RF-MEMS, then varactors.

#### 3.3 RF power dissipated

The three types of switches analysed in this paper require analogue input power. The RF power dissipated represents the ohmic losses due to switches and other ohmic factors such as dielectric losses. This power is defined as the difference between the power radiated divided by the gain and the power accepted as shown in (1). The accepted power is the difference between the incident power and the reflected one as shown in (2)

$$P_d = (P_r/G) - P_a \quad (1)$$

$$P_a = (1 - |S_{11}|^2)P_i \quad (2)$$

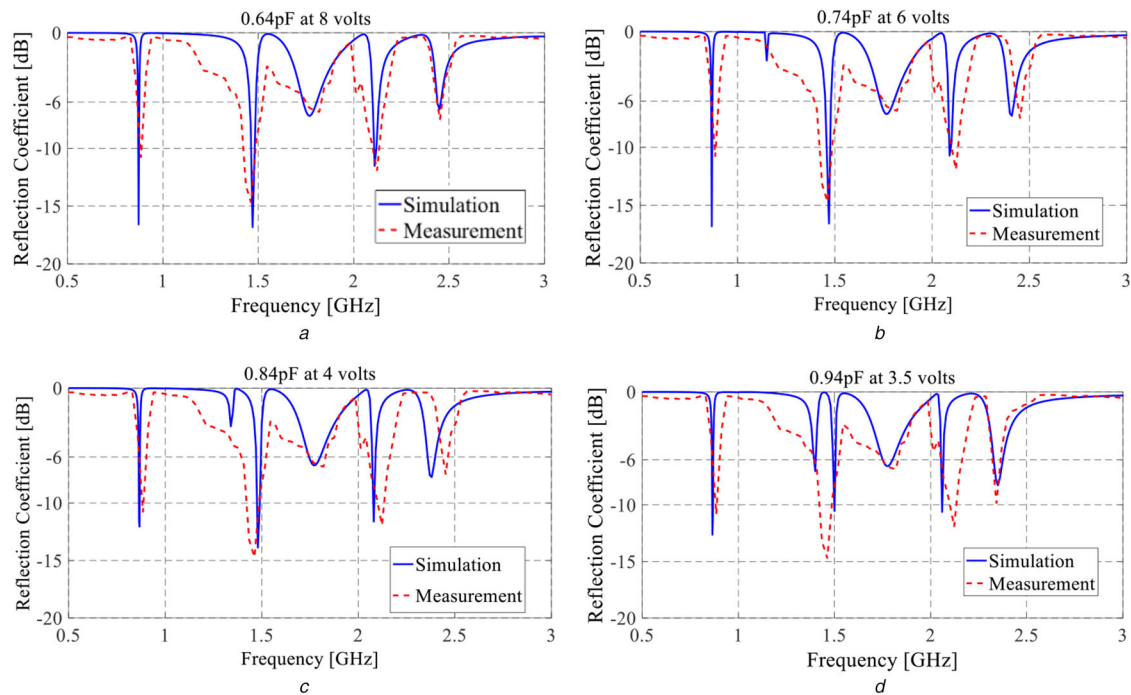


**Fig. 6** Simulated and measured reflection coefficient in dB for the various states and biasing voltages of the varactor

**Table 4** Operating frequencies for various switches configurations along with the corresponding maximum gains, radiation efficiencies and RF power dissipated for varactors

Varactor capacitance	Operating freq., GHz	Bandwidth, MHz	Max. gain, dB		Radiation efficiency, %		Power dissipated, dBm
			Sim.	Meas.	Sim.	Meas.	
0.64	0.77	6	1.3	1.23	74	78	1.06
	1.47	40	4.4	4.3	95	93	0.3
	1.775	70	4	3.98	95	93	0.26
	2.1–2.13	40	4.54	4.5	97	95	0.16
	2.44–2.46	20	3.8	3.73	93	89	0.5
0.74	0.86	6	1.2	1.1	73	76	1.16
	1.45–1.48	30	4.3	4.2	99	93	0.26
	1.73–1.8	70	3.75	3.6	97	95	0.16
	2.08–2.11	30	4.33	4.1	97	95	0.16
0.84	2.39–2.42	30	4	2.9	96	95	0.06
	0.865	10	1.2	1.1	73	79	0.96
	1.48–1.5	20	4.1	4.1	95	95	0.16
	1.75–1.8	50	3.66	3.6	98	93	0.26
	2.07–2.09	20	4.1	4	97	95	0.16
0.94	2.36–2.4	40	4	3	97	96	0.06
	0.865	10	1.2	1.1	73	76	1.16
	1.77–1.8	30	3.7	3.68	98	91	0.36
	2.06–2.07	10	3.7	3.53	95	91	0.36
	2.33–2.38	50	4.3	4	98	91	0.36

The RF power dissipated is calculated for different switches at various configurations. Since, the dielectric losses are constant for all frequencies, the variation in the power dissipated is due to the capacitance and resistance variation in the switches. In the case of a pin diode, the power dissipated ranges between 4.3 and 12.8 dBm. For the RF-MEMS, the power dissipated values vary between 2.3 and 7 dBm. In the case of varactors, the power varies between 0.06 and 1.16 dBm. Since the power dissipated represents the ohmic losses, the switch that exhibits the lowest power consumption is the varactor in this case.

### 3.4 Radiation efficiency

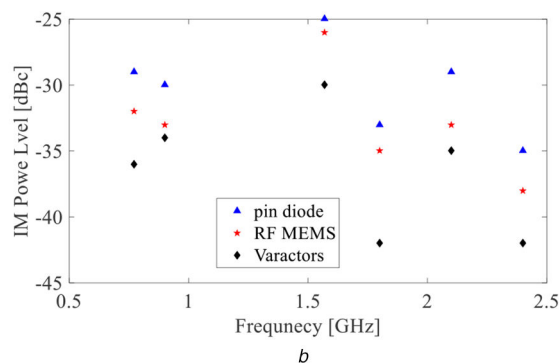
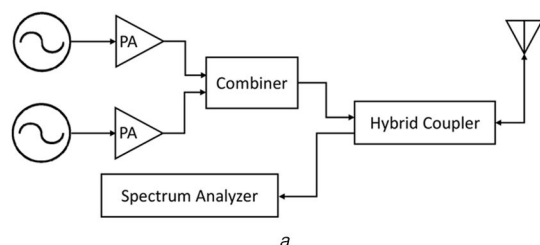
The radiation efficiency of an antenna is related to how much power can an antenna radiate with respect to a certain accepted power as shown in (3) [20]. In order to have fair comparison between different switches and over various frequencies, the

radiation efficiency is re-calculated in order to eliminate the effect of the reflection coefficient on the radiation efficiency. This is accomplished by considering a constant accepted power for the various operational frequencies. Power accepted is defined to be the input power considering the power reflected. The radiation efficiency of the antenna is measured for different switches as shown in Table 5. It is apparent that the PIN diode reconfigured PIFA displays a lower efficiency in comparison to RF MEMS and varactors' reconfigured PIFAs. The radiation efficiencies when the PIN diode is integrated ranges between 44 and 18%. For RF MEMS, the radiation efficiencies vary between 94 and 67%. In the case of a varactor integrated antenna structure, the radiation efficiencies vary between 97 and 80%

$$R_e = \frac{P_r}{P_a} \quad (3)$$

**Table 5** Radiation efficiency for various switches

Operating freq., GHz	Radiation efficiency, %		
	PIN diodes	RF MEMS	Varactors
0.87	44	67	80
1.54	32	94	95
1.8	15	94	96
2.1	28	75	96
2.4	18	94	97

**Fig. 7** PIM measurement setup and results

(a) PIM measurement setup block diagram, (b) IM power level [dBc] for different switching techniques taking  $\Delta f = 30$  MHz

### 3.5 Non-linearity

A pin diode is a semiconductor switch that has a non-linear current–voltage curve as clearly illustrated in [27]. When such a switch is integrated into an antenna structure, this non-linearity effect leads to low radiation efficiency and less radiated power in comparison with RF-MEMS and varactors. On the other hand, an RF-MEMS is an electromechanical switch that relies on a mechanical movement. It operates as a relay that closes when subjected to a voltage and opens when connected to the ground. Therefore, RF-MEMS has a linear  $I$ – $V$  performance as shown in [25] and this leads to a higher radiation efficiency, when integrated in an antenna structure. Moreover, a varactor is a semiconductor diode that relies on increasing its capacitance value by increasing the depletion region, which increases when reverse voltage is applied. The variation of the capacitance values occurs based on the change in the reverse bias. Since the varactor requires reverse voltage, the current will be near zero for all voltage values. Therefore, a varactor has a linear  $I$ – $V$  function as shown in [28] that can lead to a higher radiation efficiency when integrated in an antenna structure.

In addition, intermodulation (IM) characterisation is also held to study the effect of the switches non-linearity on the antenna's IM components. Such IM characterisation is executed according to the measurement setup shown in Fig. 7a. In this measurement setup, two signals are generated at frequencies  $(f + \Delta f)$  and  $(f - \Delta f)$ , respectively.  $f$  is the frequency of operation of the antenna and  $\Delta f$  is taken to be 30 MHz. For the pin diode case, the biasing voltage is taken as 1 V. The frequencies are 770 MHz, 1.8 GHz and 2.1 GHz when S1 is OFF and S2 is ON; 900 MHz and 2.4 GHz when S1 is OFF and S2 is OFF; 1.54 GHz when S1 is ON and S2 is ON. For the RF MEMS, the biasing voltage is taken as 2.75 V. The frequencies are 1.54 and 2.4 GHz when M1 is OFF and M2 is OFF; 770 MHz and 1.8 GHz when M1 is OFF and M2 is ON; 900 MHz and 2.1 GHz when M1 is ON and M2 is OFF. For the varactors case, the biasing voltage varies from 1 to 6 V depending on the desired capacitance value. The frequencies are 770 MHz, 1.8 GHz and 2.1 GHz when the varactor capacitance is 0.64 pF; 900 MHz and 2.4 GHz when the varactors capacitance is 0.74 pF; 1.54 GHz when the varactor capacitance is 0.84 pF. The two signals are amplified by relying on two power amplifiers and then fed into a power combiner. The combined output signal is then fed into a hybrid coupler. The output of the hybrid coupler is connected to the antenna under test, while the coupling port is fed into a spectrum analyser. It is important to note that all instruments and devices are

calibrated before usage. Fig. 7b, shown below, displays the intermodulated power level subtracted from the power level at the fundamental frequencies. It is concluded according to the finding of Fig. 7 that all the PIFA antennas show a considerably low IM power that is expressed in dBc in Fig. 7b as a function of frequency and for different switching techniques. Such performance is expected due to the optimised and low number of switches in the all the PIFA configurations.

### 3.6 Reliability

The mechanism governing the operation of PIN diodes and varactors is based on the high-level injection of electrons. Therefore, when PIN diodes or varactors are used as switches in antennas, they offer a higher reliability, better mechanical ruggedness and faster switching speed than electro-mechanical designs. Skyworks application notes [26–28] prove the high reliability of pin diodes and varactors. However, numerous studies are held in order to address the reliability of RF MEMS [29]. The friction effects between the metal to metal [resistive switches or metal to insulator contacts (capacitive case)] must be alleviated for an improved RF MEMS reliability [29].

### 3.7 Bandwidth

Bandwidth is an important criterion to measure in an antenna design performance appraisal. As shown in Table 6, for pin diodes, the antenna is able to cover only the uplink or downlink channels of the design. For the case of RF MEMS, the antenna can cover the uplink and some of the downlink channels. However, for the case of varactors, the tunable performance allows the operation over a larger bandwidth and thus enables covering all the uplink and downlink channels for all desired applications.

### 3.8 Testing on another antenna type

The conclusions drawn from our analysis, simulations and experimentation of the presented reconfigurable PIFA antenna are also tested for verification on another antenna. A typical circular patch antenna, presented in [30] is reconfigured by relying on a digital tunable capacitor (DTC). For the sake of verification and proof of concept, the DTC is replaced with a PIN diode, RF MEMS and a varactor, respectively. The same analysis is executed across the reconfigurable circular patch for all different reconfiguration techniques and the conclusions drawn are in line with the results presented herein in Sections 1 and 2. Table 7

**Table 6** Bandwidth comparison between different switches

Switch state	Operating freq., GHz	Bandwidth, MHz
S1 OFF and S2 OFF	0.9	10
	1.8	50
	2.4	20
S1 OFF and S2 ON	0.77	10
	1.54	30
	1.8	40
	2.66	70
	5.2	60
S1 ON and S2 OFF	1.8	40
	2.1	30
	3.55	70
	5.2	60

Switch state	Operating freq., GHz	Bandwidth, MHz
M1 OFF and M2 OFF	1.54	20
	2.4	100
M1 OFF and M2 ON	0.77	10
	1.54	20
	1.8	40
	2.66	90
M1 ON and M2 OFF	0.9	12
	1.54	40
	1.8	70
	2.1	60

Varactor capacitance	Operating freq., GHz	Bandwidth, MHz
0.64	0.77	6
	1.47	40
	1.775	70
	2.1–2.13	40
	2.44–2.46	20
0.74	0.86	6
	1.45–1.48	30
	1.73–1.8	70
	2.08–2.11	30
0.84	2.39–2.42	30
	0.865	10
	1.48–1.5	20
	1.75–1.8	50
0.94	2.07–2.09	20
	2.36–2.4	40
	0.865	10
	1.77–1.8	30
	2.06–2.07	10
	2.33–2.38	50

presents the results obtained for the antenna of [30]. Such results validate the discussion presented herein and enable the scalability of this analysis.

#### 4 MIMO implementation of the reconfigurable PIFA system

The reconfigurable PIFA design presented in Section 2 is now proposed for integration as part of a two-element MIMO system. Such MIMO implementation is instrumental in a heavily loaded and connected environment. The MIMO system will be evaluated with the three reconfiguration techniques.

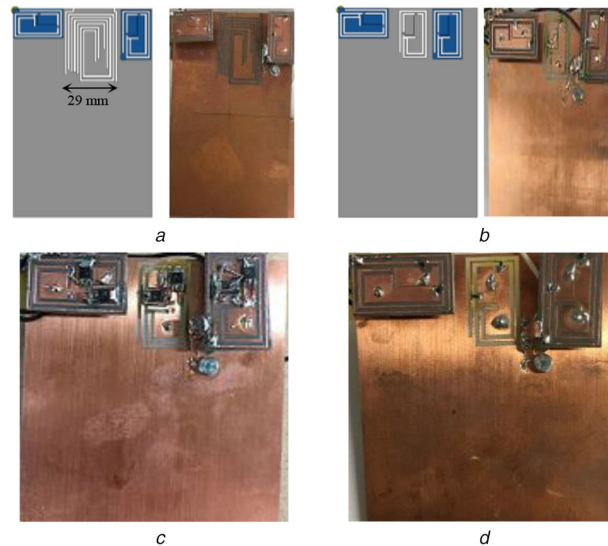
#### 4.1 MIMO system evaluation basics

In order to verify that a MIMO configuration is successfully implemented and can be integrated into a mobile device, certain parameters must be verified. The first parameter that must be studied is the envelope correlation coefficient. It is a measure of the dependency of the radiation patterns of the various antenna elements in a MIMO system on each other [31]. It can be represented as shown in the following equation:

$$\rho_e = \frac{|\iint \overline{F}_1 \cdot \overline{F}_2^* d\Omega|^2}{\iint |\overline{F}_1|^2 d\Omega \iint |\overline{F}_2|^2 d\Omega} \quad (4)$$

**Table 7** Performance analysis of the antenna in [30] when reconfigured with PIN diode, RF MEMS and varactor

Reconfiguration technique	Frequency, GHz	Gain, dB	Radiation efficiency, %	Power dissipated, dBm	Biassing, mW
PIN diode	2.4 when ON	2.7	47	21	5
	2.6 when OFF	2.8	60		
RF MEMS	2.7 when ON	3	62	4	85
	2.8 when OFF	3.1	72		
Varactors	starting tuning 2.6	3.2	82	0.5	125
	ending tuning 2.5	3.3	91		

**Fig. 8** Implementation of MIMO reconfigurable antenna prototypes

(a) Using PIN diodes and multiband reject slots, (b) Using varactors and reconfigurable varactor-based band reject, (c) Using RF-MEMS, (d) Using PIN diodes

In (4),  $F_1$  and  $F_2$  represent the radiation patterns of both antennas [31]. The MIMO system performance can be evaluated as acceptable if the envelope correlation coefficient of the antenna system is  $<0.5$  at the desired operational frequencies.

The second parameter that must be checked is the isolation. It evaluates the coupling that exists between the various antenna ports. For a well-designed MIMO system, the isolation must remain less than  $-15$  dB. The total active reflection coefficient is also a significant MIMO parameter that must be verified. The active reflection coefficient of the antenna elements measures the reflected power from the total incident power while taking into consideration the coupling that exists between the various antenna elements as shown in the following equation [31]:

$$\Gamma_a' = \frac{\sqrt{\sum_{i=1}^N |b_i|^2}}{\sqrt{\sum_{i=1}^N |a_i|^2}} \quad (5)$$

The various 'a' and 'b' represent the incident and reflected signals, respectively, at the various ports [31]. For an acceptable MIMO performance, the total active reflection coefficient must remain less than  $-10$  dB at the operating frequencies for a typical antenna and less than  $-6$  dB for antennas that are proposed for mobile devices.

The mean effective gain (MEG) must also be verified for a complete MIMO analysis. MEG is a statistical measure of the antenna gain in a mobile environment. It is defined by the ratio between the mean received power of the antenna and the total mean incident power when moving the antenna over a random route [31]. It can be expressed mathematically as shown in the following equation:

$$\text{MEG} = \int_0^{2\pi} \int_0^\pi \left( \frac{\text{XPR}}{1 + \text{XPR}} G_\theta(\theta, \varphi) P_\theta(\theta, \varphi) + \frac{1}{1 + \text{XPR}} G_\varphi(\theta, \varphi) P_\varphi(\theta, \varphi) \right) \sin \theta d\theta d\varphi \quad (6)$$

In (6), XPR is the cross-polarisation power ratio, and  $P_\theta$   $P_\varphi$  are the theta and phi components of the normalised angular power density functions of the incoming plane waves [20]. These waves are presented in this work by Gaussian distribution in an indoor and outdoor environment. In order to verify that a MIMO system is suitable for implementation, the ratio between the MEGs for the two antenna elements must be close to one, i.e.  $\text{MEG1}/\text{MEG2} \approx 1$ .

The final parameter that will be considered for MIMO analysis is the diversity gain (DG). It represents the true benefit of the diversity scheme towards a single-antenna system. It is defined to be the difference between the signal-to-noise ratio (SNR) of the combined signals of all the radiators of a multi-antenna system and the SNR of the best single antenna of the structure as presented in the following equation:

$$\text{DG} = [\text{SNR}_{\text{combined}} - \text{MAX}(\text{SNR}_{\text{barncchi}})] \quad (7)$$

#### 4.2 Design of a reconfigurable MIMO PIFA system with a multiband reject filter for isolation enhancement

The MIMO system topology is composed of two reconfigurable PIFA elements that are positioned perpendicular to each other. The reconfigurable antenna elements are separated by a distance of 29 mm as indicated in Fig. 8a. The multiband resonating structure is composed of six nested capacitive slots that are incorporated into the ground plane of the entire antenna system. The basic mathematical equation that is employed for this design is the use of an  $L = \lambda/2$  resonator incorporated into the ground plane. This resonator can be repurposed to act as a band reject filter as discussed in [32]. The transformation of the stub into a  $\lambda/2$  slot etched from the ground plane of a radiating structure is based on Babinet's principle [20]. The slot etched from the ground plane behaves as a mean to reject undesired bands and hence it behaves as a band reject filter for isolation enhancement in the MIMO system.

The lengths of these band reject  $\lambda/2$  slots are then optimised in order to account for the capacitive coupling among each other. Hence, these slots act as a multi-band reject filter and improve the

isolation levels between the two elements of the whole MIMO system. Table 8 presents the correlation between the lengths of the slots and their resonances. The isolation improvement at the various frequencies of operation is shown in Fig. 9. This graph compares the isolation between the antenna elements with and without the presence of the different nested slots. It is shown that the isolation is clearly improved at the frequencies 770 MHz, 900 MHz and 2.66 GHz while no improvement is noticed at 1.8 GHz. This lack of improvement at 1.8 GHz is an indicator that the band reject filter design must be improved in order to ensure isolation enhancement at all frequencies of interest. In the next section, the reconfiguration of the band reject filter is proposed alongside the reconfigurable antenna elements to improve the isolation at all the desired frequencies of operation.

#### 4.3 Reconfigurable isolation using varactors

In this section, the nested slots filter is reconfigured in order to reject and improve the isolation in accordance with the reconfigurable antenna elements' operation. The reconfigurable band reject filter is composed of three layers as shown in Fig. 10a. The first layer is a 50  $\Omega$  transmission line of 70 mm length. The second layer is a Rogers substrate RO5880 of 1.6 mm thickness and 2.2 dielectric constant. The third layer is the ground plane where a rectangular spiral slot is etched. The spiral slot is centred below the 50  $\Omega$  transmission line. The spiral shape of the slot is intentional in order to reduce the needed landscape and achieve a more compact design. Several current paths can be achieved within the spiral slot structure as highlighted in Fig. 10b. Each path corresponds to half wavelength at a frequency of interest in order to achieve the needed band rejection. The first path represents a  $\lambda/2$  stub at 900 MHz. The second and third paths correspond to  $\lambda/2$  slots at 2.1 and 2.4 GHz, respectively. These paths can be represented by second-order LC equivalent circuits as shown in Fig. 10c. The inductance and capacitance values depend on the slot impedance and the frequency bands. The values can be calculated according to (8) and (9) [32]. Table 9 represents the inductance and capacitance values of the proposed equivalent circuit. The detailed dimensions of the slots are shown in Fig. 10d. The overall design dimension of the filter's substrate is 70  $\times$  30 mm<sup>2</sup>. Fig. 11 shows the transmission and reflection coefficients of the proposed LC equivalent circuit along with the proposed filter design. Both datasets exhibit the same band reject frequencies at 900 MHz, 2.1 GHz and 2.4 GHz. Such results prove that the equivalent circuit model represents closely the proposed filter design.

Reconfiguring the performance of the proposed band reject filter can be achieved by integrating a varactor and a resistor at specific locations along the slot. Their positions are chosen such that the effective length of the slot along with the equivalent effect of the varactor result in a band reject behaviour at the desired frequency bands

$$L = \frac{Z_o(f_2 - f_1)}{\pi f_1 f_2} \quad (8)$$

$$C = \frac{1}{4\pi Z_o(f_2 - f_1)} \quad (9)$$

where  $Z_o$  is the line impedance;  $f_1$  is the lower cut-off frequency;  $f_2$  is the upper cut-off frequency.

The reconfigurable filter topology along with the integrated varactor and resistor is shown in Fig. 10d. By varying the biasing voltage that is supplied to the integrated varactor, a reconfigurable band rejection is achieved over different communication frequencies. These frequencies are 900 MHz, 1.54 GHz, 1.8 GHz, 2.1 GHz and 2.4 GHz accordingly. The presented filter relies on the SMV1247-079LF varactor [26]. Its capacitance changes from 8.86 to 0.64 pF with a varying input voltage from 0 to 8 V. Mainly, by biasing the varactor with different voltages, the corresponding current path changes depending on the capacitance variation. This enables the band rejection of the filter to occur at multiple desired frequencies. Similar LC equivalent circuit models can be derived for the reconfigurable filter by considering the electrical model of

the integrated varactor. Fig. 12 shows the fabricated reconfigurable band reject filter. Two 110 nH RF S are introduced to connect the varactor to the DC power supply as shown in the fabricated prototype in Fig. 12a. The RF chokes prevent any RF leakage from the filter towards the DC biasing circuit through the two embedded vias. Fig. 12b shows the integration of the varactor and the resistor along the slots in the ground plane of the filter. The effect of varying the varactor's capacitance on the transmission coefficient of the filter is shown in Fig. 13a for the span of frequencies from 0.8 to 1 GHz while Fig. 13b is dedicated for the 1.5–2.5 GHz range. The filter is able to tune its band reject behaviour based on the capacitance of the varactor. It is important to note that the reflection coefficient at each corresponding band reject frequency is maintained as close as possible to 0 dB. Fig. 9b shows the MIMO system with the varactor integration on the band reject filter and the antenna elements. Table 10(c) and Table 11(c) present the envelope correlation coefficient and the MEG calculation. The isolation improvement is represented in Fig. 9. As seen, the MIMO system criteria is met since the correlation coefficient is <0.5, the isolation is bigger than 15 dB and all the MEG ratios are around one. Fig. 14c shows the active reflection coefficient of the MIMO system. The DG is found to be around 10 dB for the various varactors configurations.

#### 4.4 MIMO implementation using PIN diodes

The band reject filter in this case is reconfigured using two PIN diode switches as shown in Fig. 8b, similarly to the two antenna elements. The MIMO performance evaluation in terms of envelope correlation coefficients is shown in Table 10(a). It is clear that this MIMO system meets the isolation and correlation coefficient requirements where all correlation coefficients are <0.5 and the isolation is maintained below -15 dB for all operational frequencies as shown in Fig. 9. The MEG results are presented in Table 11(a), where the MEG ratio is maintained at  $\sim 1$  for all frequencies of interest. Fig. 14a represents the active reflection coefficient for all switches' configurations. The results indicate that the antennas in the MIMO system are fully functional at the required frequencies. Fig. 15 shows the DG that is equal to 10 dB when only S1 is ON. The DG varies between 10 and 10.5 dB for other switches configurations. This highlights the benefit of the diversity scheme towards a single-antenna system.

#### 4.5 MIMO implementation using RF MEMS

In this part, the same MIMO system is implemented where pin diodes are replaced by RF-MEMS. Fig. 8d represents the RF-MEMS based MIMO system prototype. The band reject filter in the ground is now reconfigurable using two RF-MEMS. The improvement in the isolation is included in Fig. 9. Table 10(b) shows the envelope correlation coefficient results for different switch configurations. Similar to pin diodes, the correlation coefficient and the isolation show good results. The MEG results are presented in Table 11(b). Fig. 14b represents the active reflection coefficient of the different configurations. The DGs range between 10 and 11 dB for various switches' configurations. These results validate that an RF-MEMS based reconfigurable antenna system satisfies the MIMO requirements under various conditions.

#### 4.6 Impact of switches on MIMO system performance

Analysing the performance of the MIMO system in function of the reconfiguration technique implemented reveals several factors that can push an antenna designer in one direction or the other, especially when it comes to future mobile devices in an IoT era. It is found that the proposed reconfigurable PIFA based MIMO system with varactors display lower envelope correlation coefficient and a higher isolation than that of RF-MEMS and pin diodes.

In fact, such enhanced isolation performance presents the MIMO antenna system as a robust component that is suitable for integration in a system where multiple antenna components must co-exist within a limited landscape. Such scenario benefits from

**Table 8** Length of the multiband slots versus its operational frequency

Slot	Length, mm	Operational frequency, GHz
a	36.5–0.45λ	3.55
b	156.3–0.469λ	0.77
c	141–0.495λ	0.9 <sup>a</sup> and 1.8
d	69–0.56λ	2.1
e	54–0.5λ	2.4

<sup>a</sup>0.9 is taken as the lambda λ in this case.

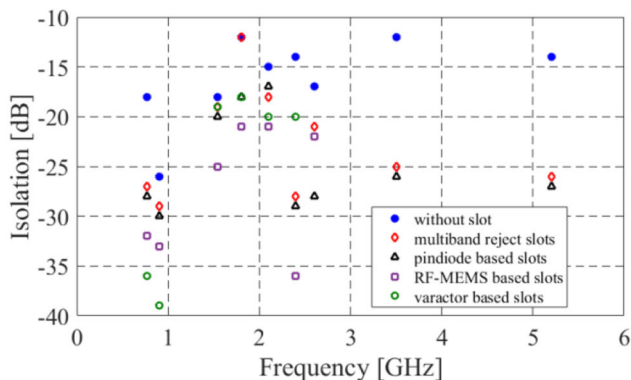


**Fig. 9** Comparison in isolation values between the various operating frequencies at the different elements' configurations

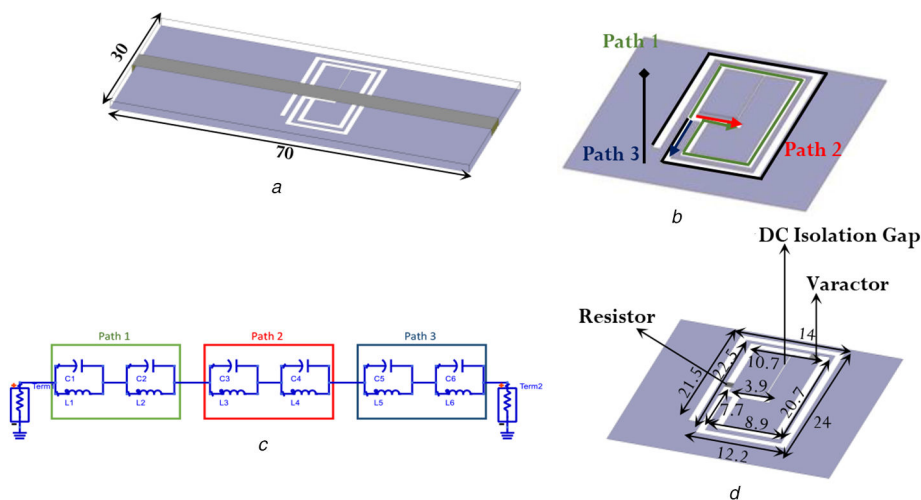


**Fig. 10** Filter design and implementation

(a) Filter topology, (b) Current paths before the addition of any active component, (c) Equivalent LC circuit model of the presented filter, (d) Detailed dimensions of the various slots along with the location of the integrated varactor and resistor

**Table 9** Inductance and capacitance values for the three current paths

	Inductance, nH		Capacitance, pF
L1 = L2	0.251	C1 = C2	136
L3 = L4	0.133	C3 = C4	42
L5 = L6	0.719	C5 = C6	6.2

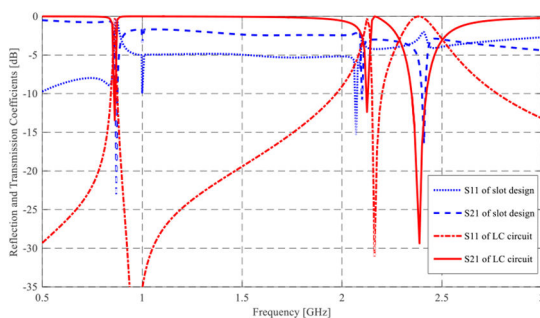


**Fig. 11** Comparison between the transmission and reflection coefficients of the proposed LC equivalent circuit and the filter 3D structure

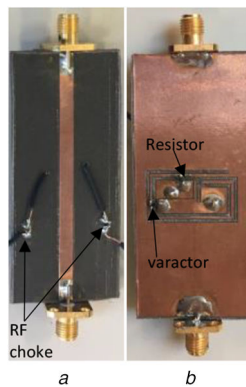


**Fig. 12** Reconfigurable band reject filter prototype  
(a) Front side, (b) Bottom side

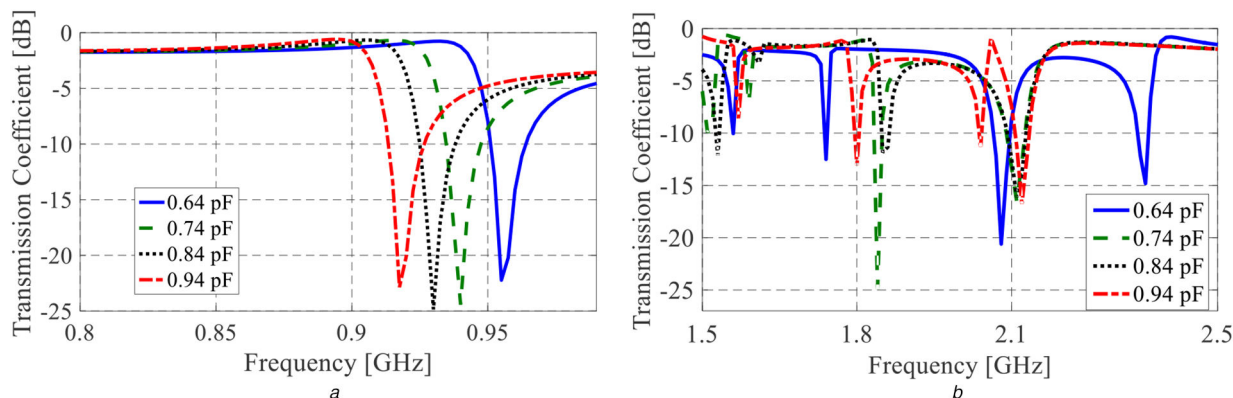


**Fig. 13** Variation of the transmission coefficient in dB for various varactor capacitance values  
(a) Between 0.8 and 1 GHz, (b) Between 1.5 and 2.5 GHz

**Table 10** Envelope correlation coefficient with PIN diode integration, RF-MEMS and varactors

(a) PIN diode integration			
Switch state	Op. freq., GHz	Correlation coefficient	
	Sim.	Meas.	
S1 OFF and S2 OFF		0.9	0.1854
		1.8	0.5
		2.4	0.5
S1 OFF and S2 ON		0.77	0.027
		1.54	0.3
		1.8	0.0298
		2.66	0.005
S1 ON and S2 OFF		1.8	0.14
		2.1	0.009
S1 ON and S2 ON		0.77	0.021
		1.54	0.31
		1.8	0.03
		2.1	0.009

the reconfigurable isolation performance to enhance its operation. In addition, the choice of a reconfiguration technique to be implemented within the system can be a determining and impactful factor on the successful implementation of such a system in a practical scenario. One must also note that the difference in the MIMO system's performance is also due to the difference in the single antenna element's characteristics. The number of switches in the varactor-based reconfigurable MIMO system is a total of three (one per antenna element and one for the isolating filter) rather than six (two for each antenna element and two for the isolating filter) as in the case of RF-MEMS and pin diodes. Table 12 summarises the comparative analysis executed in this paper. It is significant to note that this analysis does not compare an ON/OFF switching technique (pin diode and RF MEMS) over a tunable one (varactors). However, it aims to compare the radiating performance

of the full MIMO system when integrating different switching techniques in terms of gain, radiation efficiency, dissipated power and other parameters. It can be concluded that no switch can have an ideal (no effect) on the antenna performance, and hence the MIMO behaviour. In other words, no switch is flawless. The choice of a switch is dependent on the designer's constraints. Thus, the determination of the type of switch needed at the earlier stages of the design is a necessity, whose importance increases with the increase of the number of required antenna elements in a mobile communicating terminal. However, as shown in Fig. 8, reconfigurable isolation enhances the performance of the MIMO system itself and improves its ability to better mitigate interference.

Table 13 presents a detailed comparison between literature and the proposed work. It is immediately noted from Table 13 that the system proposed in this paper is superior to other work in literature

(b) RF-MEMS				
Switch state	Op. freq., GHz	Correlation coefficient		
		Sim.	Meas.	
M1 OFF and M2 OFF	1.54		0.38	0.3
	2.4		0.08	0.02
	0.77		0.098	0
M1 OFF and M2 ON	1.54		0.07	0.02
	1.8		0.06	0
	2.66		0.008	0.05
	0.9		0.0786	0.3
M1 ON and M2 OFF	1.54		0.127	0.12
	1.8		0.007	0
	2.1		0.223	0.45
	1.8		0.05	0.055
M1 ON and M2 ON	2.4		0.09	0.092

(c) Varactors				
Varactor cap.	Op. freq., GHz	Correlation coefficient		
		Sim.	Meas.	
0.64	0.77		0.027	0.01
	1.47		0.15	0.08
	1.775		0.086	0.07
0.74	2.1		0.12	0.11
0.84	0.9		0.03	0.04
0.94	2.4		0.09	0.1

**Table 11** MEG ratios with PIN diode integration, RF-MEMS and varactors

(a) PIN diode integration				
Switch state	Op. freq., GHz	Gaussian		
		In	Out	
S1 OFF and S2 OFF	0.9		0.8	0.97
	1.8		0.94	0.9
	2.4		0.92	0.86
S1 OFF and S2 ON	0.77		0.95	0.96
	1.54		0.98	0.91
	1.8		0.86	0.87
	2.66		0.8	0.8
S1 ON and S2 OFF	1.8		0.85	0.91
	2.1		0.95	0.95
	0.77		0.95	0.965
S1 ON and S2 ON	1.54		0.98	0.905
	1.8		0.86	0.87
	2.1		0.96	0.95

in terms of agility, dynamic isolation enhancement and compact size. This is to our knowledge the first of a kind reconfigurable MIMO system with dynamic isolation that is fitted towards the frequency of operation. In addition, it is the first of a kind MIMO design process, where the impact of the reconfiguring component is also taken into consideration during the design process.

## 5 Conclusion

Modern wireless communications urge antenna designers for efficient, intelligent and compact RF front-ends. These systems must be integrated in portable devices while catering for many operational requirements that are dynamic and continuously changing on demand. Therefore, in this paper a novel reconfigurable, two-element, MIMO PIFA antenna system is analysed with multiple switching components. The MIMO system operates at a multitude of frequencies corresponding to a desired set of communication application.

In addition, the proposed MIMO system reconfigures band rejection between the radiating elements in order to enhance isolation. The impact of reconfiguring components on the system's performance and requirements is detailed. The system is analysed, simulated and measured when PIN diodes, RF MEMS or varactors are incorporated. Conclusions are drawn onto the effect and impact of switch reconfigurable MIMO PIFA system's integration in a mobile or portable device while taking into consideration various design constraints.

## 6 Acknowledgment

The authors acknowledge the support of the American University of Beirut Research Board.

(b) RF-MEMS				
Switch state	Op. freq., GHz	Gaussian		
		In	Out	
M1 OFF and M2 OFF	1.54	0.95	0.89	
	2.4	0.88	0.89	
M1 OFF and M2 ON	0.77	0.9	0.85	
	1.54	0.88	0.91	
	1.8	0.82	0.96	
	2.66	0.86	0.8	
M1 ON and M2 OFF	0.9	0.91	0.97	
	1.54	0.86	0.93	
	1.8	0.83	0.97	
	2.1	0.97	0.9	
M1 ON and M2 ON	1.8	0.83	0.95	
	2.4	0.89	0.9	

(c) Varactors			
Op. freq., GHz	Indoor		Gaussian
			Outdoor
0.87	0.8		0.78
1.54	0.8		0.9
1.8	0.8		0.8
2.1	0.82		0.8
2.4	0.8		0.8

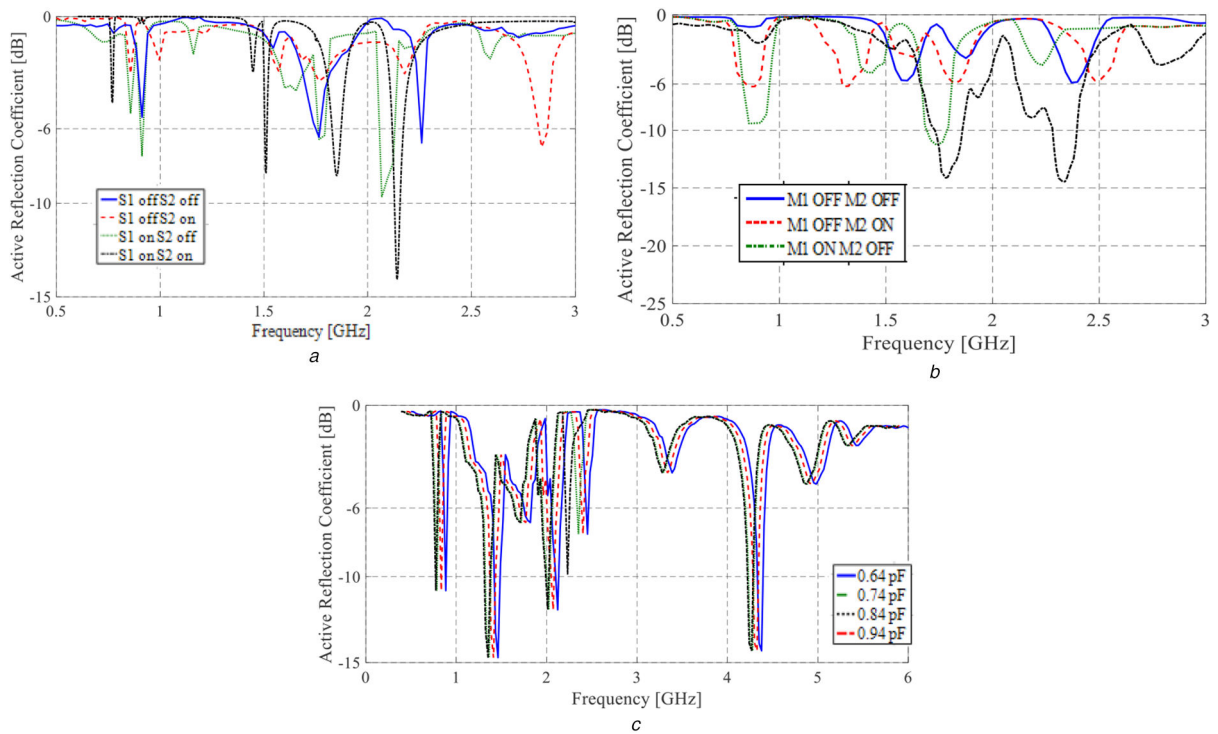


**Fig. 14** Active reflection coefficient for the various configurations of the MIMO system with (a) PIN diodes, (b) RF-MEMS, (c) Varactors

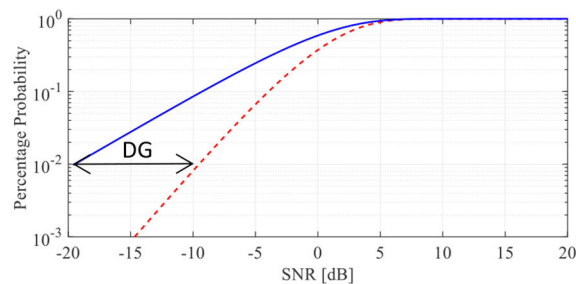


**Fig. 15** DG when S1 is ON and S2 is OFF at 2.1 GHz

**Table 12** Comparative analysis between PIN diodes, RF MEMS and varactors

Analysis	Pin diodes	MEMS	Varactors
no. of switches per antenna	two switches	two switches	one varactors
biasing (input dc power)	low dc power requirement (10 mW)	noticeable dc power requirement (171 mW)	high dc power requirements (250 mW)
power dissipated (dBm)	high ohmic losses (53–12.8 dBm)	moderate ohmic losses (23–52 dBm)	lowest ohmic losses (0.06–1.16 dBm)
radiation efficiency	low radiation efficiency (18–44%)	considerably high radiation efficiency (67–94%)	high radiation efficiency (80–99%)
non-linearity	non-linear	more linear	considerably linear
reliability	reliable	non-reliable	reliable
correlation and isolation	acceptable	acceptable	low

**Table 13** Comparison between the proposed MIMO systems with recent literature

Paper	No. of frequencies	Frequency, GHz	Decoupling structure	Antenna type	Edge to edge spacing	Enhancement, dB
[10]	1	5.8	isolator	1 × 2	0.18λ	19.6
[11]	2	2.6–2.8 and 3.4–3.6	none	2 × 2	0.5λ × 0.43λ	20
[12]	1	3.5	coupled-line resonator	1 × 2	0.07λ	26.2
[13]	1	2.45	ADS	1 × 8	0.081λ	15
[14]	1	5.8	interdigital lines	1 × 3	0.07λ	30, 8.5, N/A
[15]	1	3.325	capacitive loaded loop	1 × 2	0.12λ	55
[16]	1	2.45	waveguide metamaterials	1 × 2	0.093λ	18
proposed work with pin diode	6	0.7–0.9 1.54–1.8 2.1–2.4	reconfigurable band-reject filter based on DGS	1 × 2	0.07λ	28–30 29–19 20–22
proposed work with RF MEMS	6	0.7–0.9 1.54–1.8 2.1–2.4	reconfigurable band-reject filter based on DGS	1 × 2	0.07λ	29–32 30–28 28–28
proposed work with varactors	6	0.7–0.9 1.54–1.8 2.1–2.4	reconfigurable band-reject filter based on DGS	1 × 2	0.07λ	35–38 28–19 20–32

## 7 References

- Statista - The Statistics Portal for Market Data, Market Research and Market Studies. • Statista - The Statistics Portal for Market Data, Market Research and Market Studies. [Online]. Available at: <https://www.statista.com/>. [Accessed: 15-Mar-2019]
- Trinh, L.H., Ferrero, F., Lizzi, L., et al.: 'Reconfigurable antenna for future Spectrum reallocations in 5G communications', *IEEE Antennas Wirel. Propag. Lett.*, 2016, **15**, pp. 1297–1300
- Costantine, J., Tawk, Y., Barbin, S.E., et al.: 'Reconfigurable antennas: design and applications', *Proc. IEEE*, 2015, **103**, (3), pp. 424–437
- Saeed, S., Balanis, C., Birtcher, C.: 'Inkjet-printed flexible reconfigurable antenna for conformal WLAN/WiMAX wireless devices', *IEEE Antennas Wirel. Propag. Lett.*, 2016, **15**, pp. 1979–1982
- Ji, L.Y., Qin, P.Y., Guo, Y.J., et al.: 'A wideband polarization reconfigurable antenna with partially reflective surface', *IEEE Trans. Antennas Propag.*, 2016, **64**, (10), pp. 4534–4538
- Lin, W., Wong, H., Ziolkowski, R.: 'Wideband pattern-reconfigurable antenna with switchable broadside and conical beams', *IEEE Antennas Wirel. Propag. Lett.*, 2017, **16**, pp. 2638–2641
- Kehn, M., Quevedo-Teruel, Ó, Rajo-Iglesias, E.: 'Reconfigurable loaded planar inverted-F antenna using varactor diodes', *IEEE Antennas Wirel. Propag. Lett.*, 2011, **10**, pp. 466–468
- Tawk, Y., Costantine, J., Christodoulou, C.G.: 'Antenna design for cognitive radio' (Artech House, USA., 2016)
- Costantine, J., Tawk, Y., Woodland, J., et al.: 'Reconfigurable antenna system with a movable ground plane for cognitive radio', *IET Microwaves Antennas Propag.*, 2014, **8**, (11), pp. 858–863
- Cheng, Y.-F., Ding, X., Shao, W., et al.: 'Reduction of mutual coupling between patch antennas using a polarization-conversion isolator', *IEEE Antennas Wirel. Propag. Lett.*, 2016, **16**, pp. 1257–1260
- Li, G., Zhai, H., Ma, Z., et al.: 'Isolation-improved dual-band MIMO antenna array for LTE/WiMAX mobile terminals', *IEEE Antennas Wirel. Propag. Lett.*, 2014, **13**, pp. 1128–1131
- Vishvakshnan, K.S., Mithra, K., Kalaiarasan, R., et al.: 'Mutual coupling reduction in microstrip patch antenna arrays using parallel coupled-line resonators', *IEEE Antennas Wirel. Propag. Lett.*, 2017, **16**, pp. 2146–2149
- Wu, K.-L., Wei, C., Mei, X., et al.: 'Array-antenna decoupling surface', *IEEE Trans. Antennas Propag.*, 2017, **65**, (12), pp. 6728–6738
- Qi, H., Yin, X., Liu, L., et al.: 'Improving isolation between closely spaced patch antennas using interdigital lines', *IEEE Antennas Wirel. Propag. Lett.*, 2016, **15**, pp. 286–289
- Jafarholi, A., Jafarholi, A., Jun Choi, H.: 'Mutual coupling reduction in an array of patch antennas using CLL metamaterial superstrate for MIMO applications', *IEEE Trans. Antennas Propag.*, 2019, **67**, (1), pp. 179–189
- Qamar, Z., Park, H.C.: 'Compact waveguided metamaterials for suppression of mutual coupling in microstrip array', *Prog. Electromagn. Res.*, 2014, **149**, pp. 183–192
- Asadallah, F.A., Costantine, J., Tawk, Y., et al.: 'A multiband and reconfigurable PIFA for mobile devices'. *IEEE Int. Symp. on Antennas and Propagation*, Puerto Rico, 2016

- [18] Asadallah, F.A., Costantine, J., Tawk, Y.: 'A multiband compact reconfigurable PIFA based on nested slots', *IEEE Antennas Wirel. Propag. Lett.*, 2018, **17**, (2), pp. 331–334
- [19] Asadallah, F.A., Costantine, J., Tawk, Y., *et al.*: 'Isolation enhancement in MIMO reconfigurable PIFA for Mobile devices'. European Conf. on Antenna and Propagation, Paris, 2017
- [20] Balanis, C.A.: *'Modern antenna handbook'* (John Wiley and Sons, USA., 2007)
- [21] Skyworks Inc. 'SMP1340 Series: Fast Switching Speed, Low Capacitance, Plastic Packaged PIN Diodes', SMP 1340-079LF datasheet, 2002 [Revised March 2017]
- [22] Johanson Tech. 'High Frequency Ceramic Solutions', L-07WR11KV4 T Data Sheet, 2015 [Revised March 2019]
- [23] Keysight Solutions.: Available at '[www.keysight.com](http://www.keysight.com)', Vector Network Analyzer, [Revised March 2019]
- [24] ETS-Lindgen: Available at '[www.ets-lindgren.com/products/chambers/emc-chambers](http://www.ets-lindgren.com/products/chambers/emc-chambers)', Anechoic Chamber, [Revised March 2019]
- [25] Analog Devices: 'Wideband, 40 dB Isolation at 1 GHz, CMOS 1.65 to 2.75 V, SPST Switches', ADG 901 datasheet, 1965 [Revised March 2017]
- [26] Skyworks Inc. 'SMV1247-SMV1255 Series: Hyperabrupt Junction Tuning Varactors', SMV1247-SMV1255 datasheet, 2002 [Revised March 2017]
- [27] Skyworks Inc., Application Notes: 'Design with PIN Diodes', pp. 22
- [28] Skyworks Inc.: 'SMVXX Product Brief', Application Notes, 2014, pp.5, [Revised March 2019]
- [29] Analog Devices: 'ADG9xx Wideband CMOS Switches', Application notes, 2014, pp.2, [Revised March 2019]
- [30] Asadallah, F.A., Costantine, J., Tawk, Y., *et al.*: 'A digitally tuned reconfigurable patch antenna for IoT devices'. 2017 IEEE Int. Symp. on Antennas and Propagation & USNC/URSI National Radio Science Meeting, San Diego, CA, 2017, pp. 917–918
- [31] Sharawi, M.S.: *'Printed MIMO antenna engineering'* (Artech House, USA., 2014)
- [32] Pozar, D.: *'Microwave engineering'* (John Wiley, USA., 2012, 4th edn.)